Controllable Large-Scale Transfection of Primary Mammalian Cardiomyocytes on a Nanochannel Array Platform

Lingqian Chang, Daniel Gallego-Perez, Chi-Ling Chiang, Paul Bertani, Tairong Kuang, Yan Sheng, Feng Chen, Zhou Chen, Junfeng Shi, Hao Yang, Xiaomeng Huang, Veysi Malkoc, Wu Lu,* and Ly James Lee**

***W**hile electroporation has been widely used as a physical method for gene transfection in vitro and in vivo, its application in gene therapy of cardiovascular cells remains challenging. Due to the high concentration of ion-transport proteins in the sarcolemma, conventional electroporation of primary cardiomyocytes tends to cause ion-channel activation and abnormal ion flux, resulting in low transfection efficiency and high mortality. In this work, a high-throughput nanoelectroporation technique based on a nanochannel array platform is reported, which enables massively parallel delivery of genetic cargo (microRNA, plasmids) into mouse primary cardiomyocytes in a controllable, highly efficient, and benign manner. A simple "dipping-trap" approach was implemented to precisely position a large number of cells on the nanoelectroporation platform. With dosage control, our device precisely titrates the level of miR-29, a potential therapeutic agent for cardiac fibrosis, and determines the minimum concentration of miR-29 causing side effects in mouse primary cardiomyocytes. Moreover, the dose-dependent effect of miR-29 on mitochondrial potential and homeostasis is monitored. Altogether, our nanochannel array platform provides efficient trapping and transfection of primary mouse cardiomyocyte, which can improve the quality control for future microRNA therapy in heart diseases.*

Dr. L. Chang, Prof. D. Gallego-Perez, C.-L. Chiang, T. Kuang, Dr. Y. Sheng, Dr. F. Chen, Dr. Z. Chen, J. Shi, Dr. X. Huang, Dr. V. Malkoc, Prof. W. Lu, Prof. L. J. Lee
NSEC Center for Affordable Nanoengineering of Polymeric Biomedical Devices
Ohio State University
Columbus, OH 43210, USA
E-mail: gallego-perez.1@osu.edu; lu.173@osu.edu; lee.31@osu.edu

Dr. L. Chang, Prof. D. Gallego-Perez, Prof. L. J. Lee
Department of Biomedical Engineering
Ohio State University
Columbus, OH 43209, USA

Prof. D. Gallego-Perez
Department of Surgery
Center for Regenerative Medicine and Cell-based Therapies
Ohio State University
Columbus, OH 43209, USA

Prof. L. J. Lee
Chemical and Biomolecular Engineering Department
Ohio State University
Columbus, OH 43209, USA

C.-L. Chiang, Dr. X. Huang
Department of Internal Medicine
The Ohio State University
Columbus, OH 43209, USA

P. Bertani, H. Yang, Prof. W. Lu
Electrical and Computer Engineering Department
Ohio State University
Columbus, OH 43209, USA

Dr. Y. Sheng, Dr. F. Chen, Dr. V. Malkoc, Prof. L. J. Lee
Department of Chemical and Biomolecular Engineering
Ohio State University
Columbus, OH 43210, USA

Dr. Z. Chen
College of Mechanical and Power Engineering
Nanjing Tech University
Nanjing 211800, China

DOI: 10.1002/smll.201601465

1. Introduction

Owing to its user-friendliness and high-throughput, electroporation is one of the most commonly used physical techniques for gene/drug delivery, with great potential for medical and clinical applications.[1] Compared to chemical methods, electroporation can bypass endocytosis, thus overcoming "multidrug resistance" responses from cells.[2] There is no need for cargo prepackaging.[3,4] Commercial bulk electroporation (BEP) systems have been widely used both in vitro and in vivo.[5,6] However, due to its bulk-environment where extremely high voltage is randomly applied on individual cells, BEP usually results in significant cellular damage.[5,7] Recent advances in microfluidic-based electroporation (MEP) have enabled more benign transfection at lower voltage.[8] Nevertheless, both BEP and MEP are highly dependent on additional factors downstream of poration (i.e., endocytosis, diffusion), which lead to low and variable transfection yields at the single cell level.[3,9]

BEP/MEP based transfection of electrogenic (excitable) cells also remains challenging.[10–13] The primary function of cardiomyocytes is regulation of the contraction–relaxation cycles of hearts.[14] Their self-regulated contractibility, achieved by ion channels and exchangers that control the transportation of Ca^{2+}, is highly sensitive to external electrical stimulation. In BEP and MEP, large portions of the sarcolemma are exposed to the porating electric field, which results in ion-channel overactivation and abnormal ion flux, that trigger functional disorders and apoptosis.[10,13] Although pioneering work has been conducted on designs of electroporation-assisted intracellular probes for electrical recording of cardiomyocytes cell lines (e.g., HL-1),[15] safe and efficient electroporation systems for high-throughput transfection of primary adult cardiomyocytes in vitro are currently lacking.

We recently demonstrated nanochannel electroporation (NEP) technique for living cell transfection in a highly controllable manner.[9,16] In NEP, a single cell is positioned in tight contact with a single nanochannel (100–400 nm) while cargo on the other side of the nanochannel. As the equivalent resistance of nanochannel (>100 MΩ) is significantly higher than that of cell membrane (<10 MΩ), most of the applied voltage is distributed over the nanochannel. The NEP involves benign and highly confined membrane poration (nearby the nanochannel), as well as high-voltage (>100 V) induced electrophoresis-effect, which "shoot" cargo into cytoplasm, resulting in high transfection efficiencies and dose-control capabilities. Our previous NEP systems, however, are compromised on the transfection yields due to either nanochannel design (e.g., 2D NEP)[9,17] or cell trapping methods.[18] In this work, we report manipulation and transfection of primary adult mammalian cardiomyocytes with high efficiency and cell viability on a nanochannel array platform. Our device enables high throughput parallel delivery of functional cargo (e.g., transcription factors, oligonucleotides, molecular beacons) into cells via electroporation through nanochannels. Dose of cargo can be precisely controlled by external electric field (e.g., voltage, pulse length, and pulse number). A novel "dipping-trap" approach was implemented to precisely position the cells-to-be-transfected in direct contact with the porating nanochannels in a high throughput manner. Such a method is simple and fast, without a requirement for sophisticated systems and special buffers. Our device demonstrated transfection of adult mouse cardiomyocytes with high efficiency and safety. We applied the device to investigate the dose effect of microRNAs for cardiomyocyte therapy. Currently, loss of miR-29 is known to be associated with cardiac fibrosis, providing a clinical potential therapeutic agent for cardiac fibrosis by targeting TGF-β/Smad3 signaling.[19] However, the two faces of miR-29 in cardiovascular disease step it back.[20] The deletion of mitochondrial *Mcl-1*, a main target of miR-29 in cardiomyocyte, leads to heart disorganization, inflammation, and even lethal heart failure.[21,22] Therefore, preserving *Mcl-1* and maintaining mitochondrial homeostasis is essential to the consideration of the miR-29 family in clinical application.[23] Endocytosis/diffusion based delivery, as well as poor transfection efficiency of primary cardiomyocyte (typically <5%) by liposomes and BEPs,[11,24] makes them impractical for optimizing the dosage of microRNA therapy in most applications in cardiomyocytes. In this work, miR-29 was delivered into an array of primary adult mouse cardiomyocytes on-chip, and the dose-dependent effects of miR-29 on mitochondrial potential and homeostasis of a cardiomyocyte was analyzed. The statistics, based on a large number of cells, proved quality control of clinical microRNA therapy on heart disease.

2. Results and Discussion

2.1. Precise Large-Scale Cell Positioning on Nanochannel Array

Successful nanochannel-based electroporation requires direct cellular contact with the nanochannels. We developed a simple "dipping-trap" approach for this purpose, as illustrated in **Figure 1**a. In this procedure, a microcap array (SU8 photoresist) was patterned over nanochannel array on a silicon chip (fabrication details given in Figure S1 in the Supporting Information). Each microcap consists of a "U-shape" feature that contains a front-side cup for cell entry. To enhance cell flow, the chip surface was pretreated to be hydrophilic using piranha solution and oxygen plasma (step (i), Figure 1a). For precise cell positioning, the chip, with the "U-shape" of microcap facing up, was vertically dipped-in (≈5 min) and -out of a cell suspension (≈10^6 cells mL^{-1}) in phosphate-buffered saline (PBS). Gravity and hydrodynamic forces modulated cell trapping within the microcaps, directly over top of the nanochannel outlets (step (ii)). Tailoring the geometries of the microcap array to be slightly larger than the cell size can achieve single-cell capture in a single cup, resulting in a clear cellular array on the chip surface (step (iii)). Figure 1b shows a cross-section of the chip. Trapped by the microcap, the cell contacts with the nanochannel so that it can be effectively electroporated while target biomolecules are delivered into cytosol, as illustrated in Figure 1c. Precise alignment of the microcap to nanochannel region plays a critical role in transfection efficiency. We therefore aligned each microcap to a nanochannel in photolithography (Figure 1d). We designed

small 2016,
DOI: 10.1002/smll.201601465

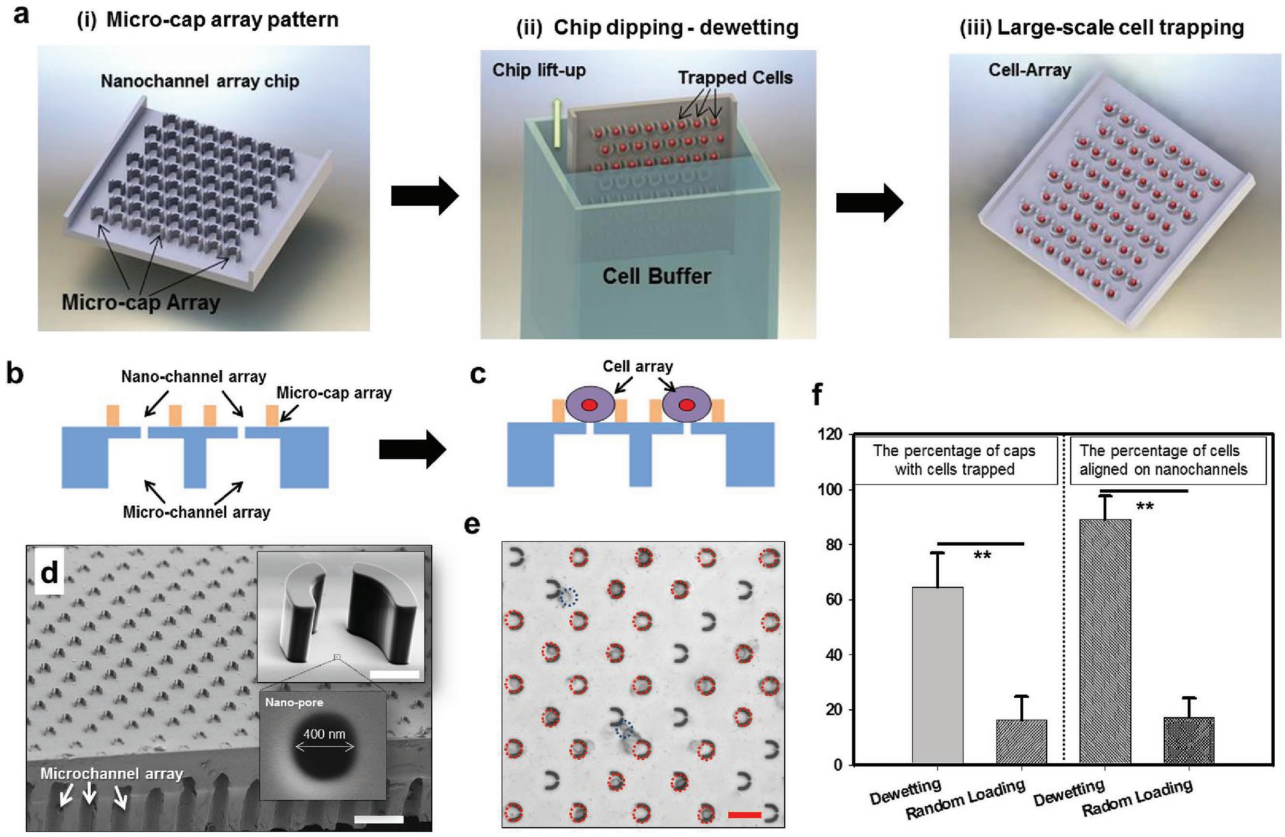

Figure 1. "Dipping-trap" method for efficient and rapid cell trapping on the nanochannel array chip. a) The schematics showing "dipping-trap" procedure for cell trapping, including i) patterning "U-shape" microcap array on chip; ii) dipping the chip into cell buffer solutions, and vertically lift-up; iii) the cells are trapped on the microcaps driven by gravities and hydrodynamics. b,c) The cross-sections of the chip before and after cells are trapped in microcaps, respectively. d) SEM micrograph of one type of microcap array ("interlaced" arrangement) patterned on the chip. The inset shows the details of one nanochannel region (single nanopore, 400 nm in diameter) which is surrounded by a single microcap. e) Cellular arrays are trapped on chip, showing single cell and single microcap pair. f) The performance of the 'dipping-trap', or 'dewetting' method with the trap-design of (d) as compared to control group (cell random loading). Two parameters are considered, including the capture efficiency (left, the percentage of microcaps with cells trapped) and the trapping specificity (right, the percentage of cells aligned on nanochannels). Scale bar: (d) 100 µm, (inset) 5 µm, (e) 50 µm. $^{**}p$-value < 0.01.

a family of microcap arrays with different dimensions and spacing to optimize the trapping efficiency (Figure 1d and Figure S2 in the Supporting Information). Our results indicate that in the "dipping-trap" procedure, microcap array with smaller geometries (width: 5 µm, spacing: 25 µm) result in low capture efficiency (≈10% microcaps with single cell trapped) but relatively high capture specificity (≈80% loaded cells aligned on the nanochannel, enabling electroporation), as shown in Figure S2c,d in the Supporting Information. In contrast, increasing the geometries (width: 10 µm, spacing: 50 µm, Figure S2a,b in the Supporting Information) is prone to clogging, which leads to low capture specificity (≈30%). Finally, we chose the "interlaced" microcap array (Figure 1d, cap width: ≈10 µm, column and row spacing: 100 µm) for subsequent experiments, which achieved remarkably high capture efficiencies and specificities (≈70%–90% and ≈90%) (Figure 1e,f).

2.2. On-Chip Massively Parallel Cargo Delivery

A high-throughput nanochannel-based transfection platform that delivers cargo into the cells patterned on the chip is illustrated in **Figure 2**a,b. Following "dipping-trap", the chip was mounted on a polydimethylsiloxane (PDMS) reservoir that contained the cargo (e.g., labeled DNA, plasmids, microRNAs). The 3D image by confocal microscopy (Figure 2c) shows that loaded cells (stained with Calcein AM, green fluorescence) are tightly in contact with individual nanochannels (white light). The nanochannel-based electroporation and its mechanism of delivery are illustrated in Figure 2d. A pulsed electric field was implemented to porate the cell membrane in contact with the nanochannel. In the meantime, the surface-charged target cargo are electrophoretically driven through each nanochannel and are delivered into the cytosol in a fast (i.e., milliseconds) and efficient manner. Physical simulation results show that due to the high equivalent resistance of the nanochannel, the biased voltage applied on single cell is relatively uniform (1.84–2.00 V) over the chip surface (1 cm^2) within a proper liquid film (e.g., 5 mm to 1 cm), in the system shown in Figure 2d. Increasing the liquid film will reduce the biased voltage across the cell (Note 1, Supporting Information). We first explored the capability of our device for massively parallel cell transfection and the "dipping-trap" approach for improvement in transfection efficiency.

DOI: 10.1002/smll.201601465

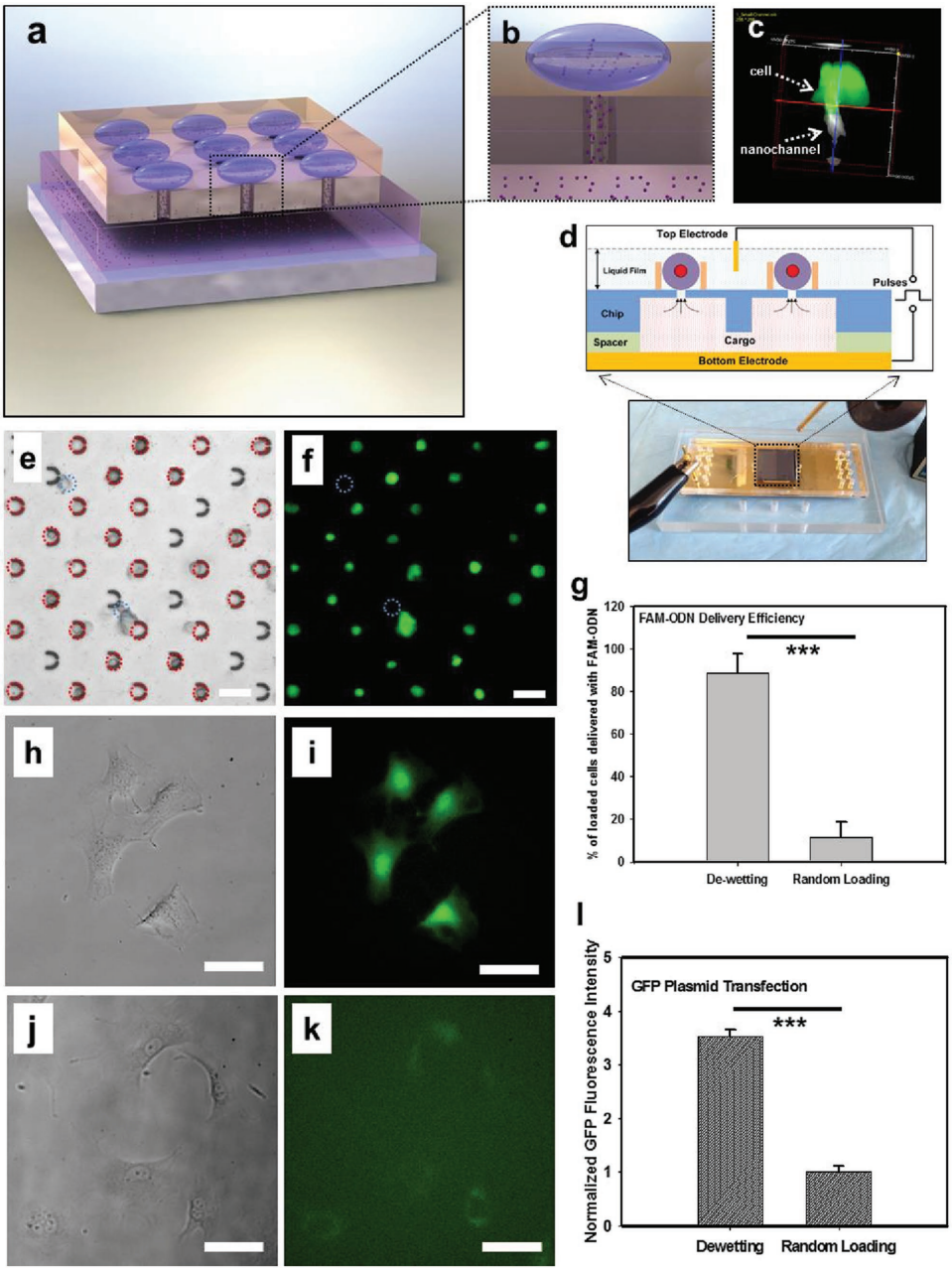

Figure 2. Massively parallel cargo delivery into trapped cells by nanochannel-based electroporation. a) The schematic of the nanoelectroporation system for *Z*-directional cargo delivery into cells trapped on the nanochannel array. b) A single cell aligned on a nanochannel is electroporated and biomolecules are delivered into the cell through the nanochannel. c) Confocal microscopy image shows a trapped cell (stain with Calcein AM, green fluorescence) tightly in contact with a nanochannel (transmission white light) which enables efficient electroporation. d) The cross-section schematic illustrates the nanochannel-based electroporation platform, consists of a bottom electrode, PDMS spacer, the chip with trapped cells, and a top electrode. Electric pulses are applied between the electrodes to electroporate the cells in the proximity of the nanochannels while electrophoretically driving the biomolecules from the bottom chamber into cells. e) Fluorescence labeled-oligonucleotides (FAM-ODN) delivered into the cells trapped on chip (labeled with red circle) result in f) obvious fluorescence. Cells "nontrapped" (indicated with blue circle) by microcaps are not delivered with ODN. g) "Dipping-trap", or "dewetting" method significantly improves the delivery efficiency as compared to random cell loading. h,i) Mouse embryonic fibroblasts (MEFs) transfected with nanochannel-based electroporation expressed GFP fluorescence. l) The nanoelectroporation assisted with the trapping method leads to significant enhancement for GFP transfection compared to control (j,k) random loading). Scale bar: e,f) 50 µm, h,i,j,k) 50 µm. ***p-value < 0.005.

Figure 2e,f shows a single-cell array (mouse embryonic fibroblasts, MEFs) is delivered with FAM-ODNs (FAM-labeled oligonucleotides) on our platform. The combination of "electrophoretic-injection" and trap-based cell patterning results in transfection efficiencies around 90%–100% (Figure 2g) compared to only ≈10% for random cell loading. Furthermore, note that the cells "off" the microcap (labeled with blue circle in Figure 2e,f) could not be transfected, thus confirming that only cells positioned to the nanochannels can be effectively porated. We next tested the performance of the device for

small 2016,
DOI: 10.1002/smll.201601465

transgenetic manipulation of living cells. MEFs were transfected with GFP plasmids (*p*-Max, 3.5 kbp) showed obvious green fluorescence expression in 6 h (Figure 2h,i; mass cell GFP expression in Figure S3 in the Supporting Information). In control group, randomly loaded cells result in weak GFP expression (Figure 2j,k). Figure 2l shows that the average GFP intensities in "dipping-trap" group are ≈6-fold higher than the control group, while showing promising uniformity (s.d. ≈3.5%). With the "dipping-trap" approach, the cells can be trapped and transfected within several minutes at a high-throughput, which is time-efficient in observing previously reported microfluidics (up to hours for high throughput),[25] optical tweezers (minutes for single-cell),[9,26] dielectrophoresis (≈30 min),[27] magnetic tweezers (≈10 min).[28,29] Moreover, the trapping protocol requires no sophisticated systems for force generation, which is simpler for clinical use.

2.3. Efficient and Controllable Gene Delivery into Adult Mouse Cardiomyocytes

The major function of adult cardiomyocytes is to orchestrate the contraction and relaxation of the heart. The contractility of a single cardiomyocyte is controlled by transmembrane ion channels (mainly, Ca^{2+}), whose functionality can be easily compromised by external electrical stimuli.[14] As such, BEP-based gene delivery to cardiomyocytes typically results in low efficiencies (≈10%),[12,30] and significant cell death due to abnormal ion flux, contraction interference, and membrane damage.[10,13] We tested the capabilities of our nanochannel-based transfection approach to deliver genes into primary cardiomyocytes in vitro in a controllable and benign manner. A high percentage of cardiomyocytes keep alive while expressing obvious fluorescence after transfection with GFP plasmids (**Figure 3**a, single cell GFP expression was shown in Figure S4 in the Supporting Information). Compared to control group (in vitro culture without treatment, see Figure S6 in the Supporting Information), the GFP intensity increased by ≈10–12-fold at 6 h post-transfection, as shown in Figure 3b. Clear GFP expression was still present after 24 h (Figure S5, Supporting Information). BEP experiments, which were also conducted for comparison purposes, resulted in low transfection efficiency and significant cell damage (Figure S6, Supporting Information). While our device yielded transfection efficiencies and cell viabilities ≈86%, BEP-based transfection led to efficiencies and viabilities of ≈5% and 13%, respectively (Figure 3c,d). MEP experiments (with channel size of 5 μm), on the other hand, did not result in clear GFP transfection and expression (Figure S6, Supporting Information), presumably due to the need for the use of low voltages (≈4 V).[29] Figure 3e demonstrates that our platform precisely control the dosage of FAM-ODN delivered into cardiomyocytes by applied voltages ranging from 0 to 200 V. Besides, the delivered dose could be controlled by the pulse durations (e.g., 5, 10, 20 ms) as well (Figure 3f). Furthermore, we demonstrated our device achieved significantly higher transfection uniformity at single-cell level than BEP, as measured by flow cytometry at high-throughput (Figure S9, Supporting Information). Altogether, our nanochannel array device demonstrated the unique capability for controllable mass cardiomyocyte transfection (>10 000 cells per chip).

2.4. Simulation of Cardiomyocytes Electroporation via Nanochannel

Observing the striking contrast between BEP and our device for transfection of primary cardiomyocytes, we next discuss the particular reason. Physical models were generated to analyze the electric fields for both nanochannel- and bulk-based electroporation at the single-cell level (**Figure 4**a–e). The electric field distribution of our device, in which two single cardiomyocytes (represented as "rectangle-shape") are localized on two nanochannels, is illustrated in Figure 4a. The simulation reveals that due to the high-resistivity of the nanochannel, among the voltage (100 V) applied in the whole system, ≈96% of the voltage drop occurs across the nanochannel, which provides high electrophoretic motility to the gene cargo during transfection. Only about 4% of the applied bias (≈4 V, Figure 4b) is directed to the cell membrane (as determined by the nanochannel diameter). Such drop is just above the transmembrane potential threshold (usually ≈0.5–1 V) needed to porate the membrane and allow cytosolic injection of the cargo. Furthermore, only a small portion of the cell membrane is exposed to the electric pulse (Figure 4c), as determined by the nanochannel size. In comparison, microchannel- or bulk-based electroporation affects significantly larger portions of the cell membrane (several μm to the whole surface), which tends to negatively compromise cell viability. With a nonspherical shape, the cardiomyocyte could be electroporated over the whole membrane instead of the poles oriented to the electric field, thus causing additional cellular damage in BEP and MEP (Figure 4d).[31] Finally, single-cell level analysis of the electric field distribution in BEP reveals significant cell-to-cell variations (Figure 4e), thus resulting in more stochastic transfection profiles compared to the more deterministic nature of nanochannel-based gene delivery.[28] In both BEP and MEP, low electric field (<50 V cm^{-1}) cannot sufficiently electroporate cells.[10,13]

2.5. Dose-Controlled Delivery Studies of miR-29 with Primary Mouse Cardiomyocytes

Loss of miR-29 expression in cardiomyocytes leads to cardiac fibrosis.[19] Although strategies aimed at replenishing miR-29 levels could offer a viable treatment for the condition, the potential side effects of this approach need to be carefully investigated. Here we used our nanochannel-based delivery platform to thoroughly evaluate the effects of precisely dosed miR-29 delivery on cardiomyocyte behavior. Normal cardiomyocytes express high miR-29, but the overexpression of miR-29 results in mitochondrial dysfunction (i.e., loss of mitochondrial potential) and cell apoptosis.[22] We delivered the gradient amount of miR-29b[32] by modulating the number of applied pulses (1–10 pulses). Tansfected cardiomyocytes were stained with JC-1 and analyzed by flow

DOI: 10.1002/smll.201601465

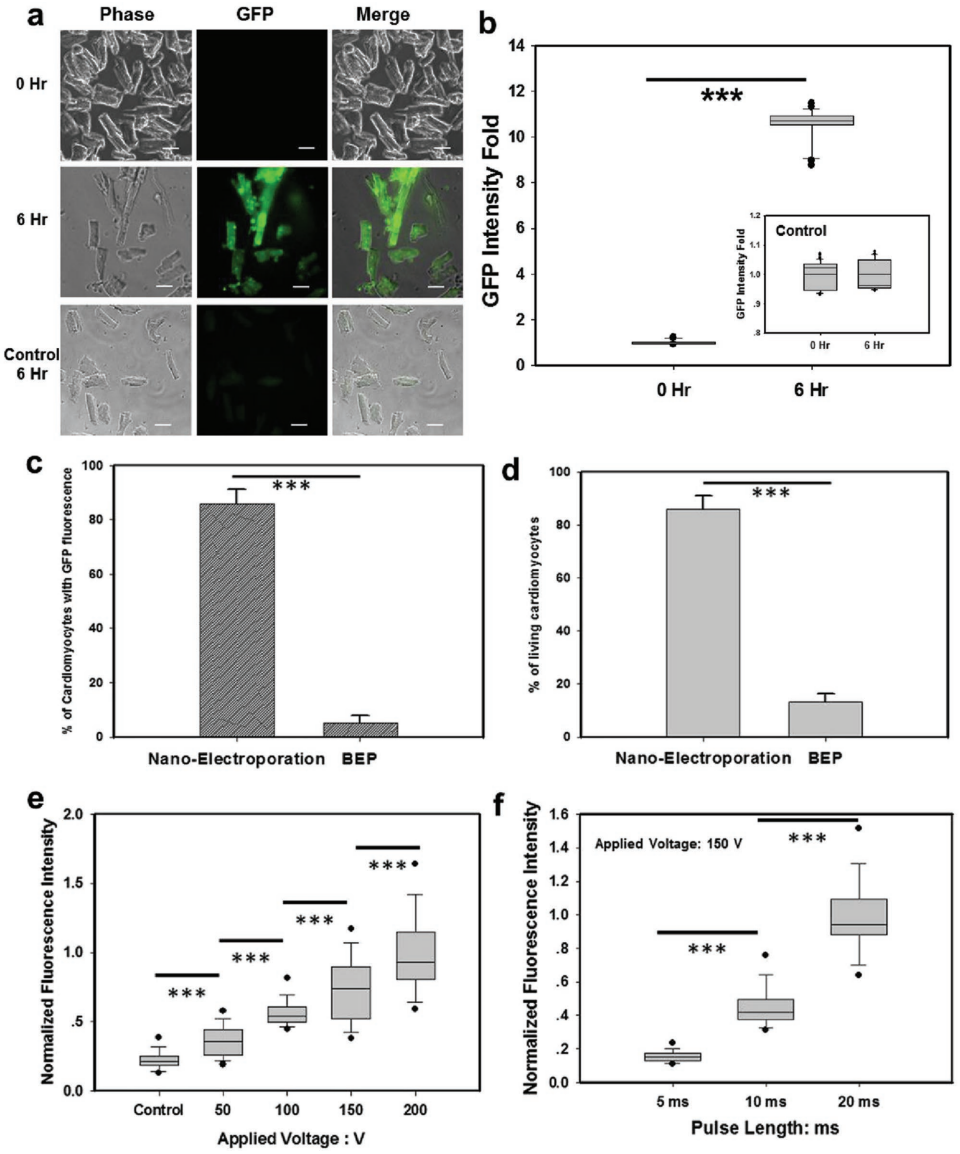

Figure 3. Safe and precise gene transfection of adult mouse cardiomyocytes on the nanochannel-based electroporation. a) Fluorescence images and b) statistics of GFP fluorescence expression 6 h after delivery of GFP plasmids (condition: 200 V, 10 ms pulse length) compared to control. Scale bar: 50 µm. c) The transfection efficiency and d) the cell viability were compared between the nanoelectroporation and BEP group. Precise dosage control can be achieved in mass cells (10 000 cells) by either e) applied voltage and f) pulse length. ***p-value < 0.005.

cytometry. JC-1 dye performs a potential-dependent accumulation in mitochondria with a fluorescence shift from green (≈529 nm) to red (≈590 nm). The ratio of red (dimer)/green (monomer) reflected to the mitochondrial potential ($\Delta\Psi$) of transfected cells (**Figure 5**a). The increasing of pulse from 0, 1, 5 to 10 significantly causes the mitochondrial depolarization and decrease in the number of high $\Delta\Psi$ cells (Figure 5b). By using the real-time PCR (polymerase chain reaction), we measured the intracellular miR-29 and its target *Mcl-1* amount post nanoelectroporation. *Mcl-1* is also highly expressed in normal myocardium, playing an essential role in myocardial homeostasis and autophagy.[22] We observed that the increased miR-29b dose could significantly suppress the *Mcl-1* expression in living cells (Figure 5c). Such a dose-dependent manner provides a hint to precisely study the threshold-dose causing the disorder of the mitochondrial homeostasis in miR-29-based gene therapy.

3. Conclusion

Primary cardiomyocytes with fully differentiated status are generally known to be difficult to transfect with nonviral approaches. Liposomal or BEP transfection of primary cardiomyocytes typically performs low efficiencies. In addition, BEP causes significant cell damage. Novel technologies capable of delivering genetic cargo to electrogenic cells in a controlled, efficient and benign manner are clearly needed in order to facilitate the development of gene therapies for cardiac tissue, and/or enable a host of critical studies of cardiac

DOI: 10.1002/smll.201601465

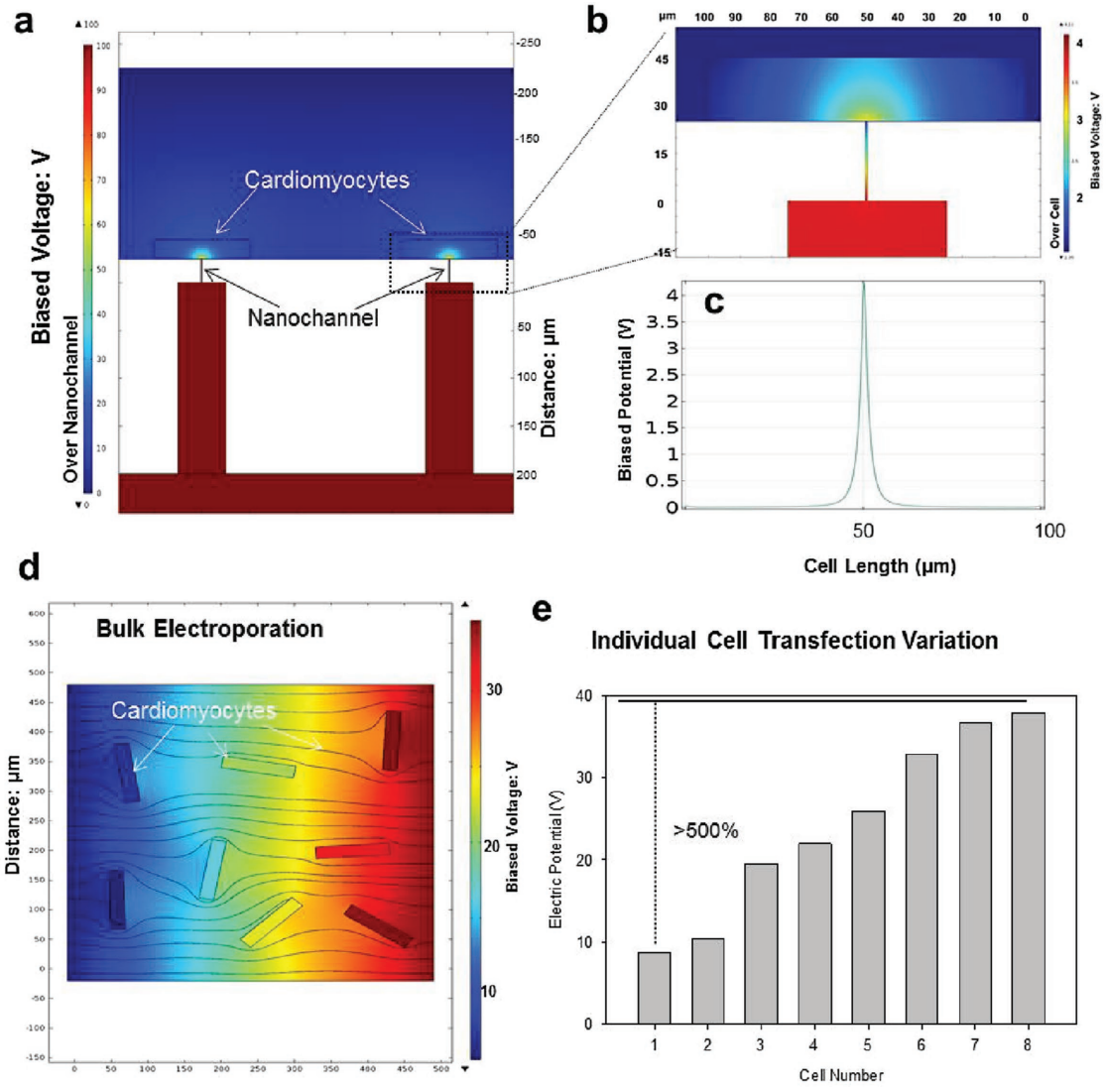

Figure 4. Physical simulations of electric fields in nanochannel- and bulk-electroporation for cardiomyocytes transfection. a) The distribution of biased voltage in nanochannel where two single cardiomyocytes are localized. b) Due to high resistivity of nanochannel, most of the applied voltage occur across the nanochannel (≈96 V), while a low potential drop (≈4 V) over the cell membrane, which is benign for single cell electroporation. c) Biased potential along the cell membrane reveals only a tiny region of the cell membrane close to nanochannel has high potential to be porated. d) In contrast, cells are electroporated stochastically in the bulk solutions in BEP, which causes e) a huge variation of biased voltages applied on individual cells.

cell biology and physiology. In this work, we reported a nanochannel array platform for large-scale single-cell trapping and on-chip transfection of primary cardiomyocytes at a high-throughput. A fluidic-based "dipping" method was developed to trap and precisely align an array of individual cells on the nanochannel chip where the electroporation condensed. Our device assisted with the trapping method demonstrated high transfection efficiencies and dosage control capabilities with single-cell resolution, which is not achievable with any existing technology. We achieved precise dosage control of miR-29 delivery in primary mouse cardiomyocyte, providing a titration of miR-29 effects on primary cardiomyocytes for further clinical application. In conclusion, our platform provides an efficient trapping and electroporation method with precise dosage control on primary mouse cardiomyocyte, which will improve the clinical microRNA therapy on heart disease.

4. Experimental Section

4.1. Nanochannel Array Chip Fabrication

The nanochannel array chip was made using a silicon wafer via clean room techniques (Figure S1, Supporting Information).[18,33] A standard double-side polished wafer (4 in., 500 μm in thickness) was first thinned to 250 μm using wet etching (45% KOH, 80 °C). A microcircle array (50 μm in diameter) was then patterned on one side of the chip using SPR220 photoresist (Dow Chemicals, US). Deep reactive ion-etch (DRIE) was applied to etch the photoresist-masked side so that a microchannel array (diameter: 50 μm; depth: 240 μm) was formed. An array of nanochannel was then patterned using AZ-5214 photoresist (Clariant Corporation, US), and DRI-etched until the nanochannels connected with the microchannels. In our experiments, each chip,

DOI: 10.1002/smll.201601465

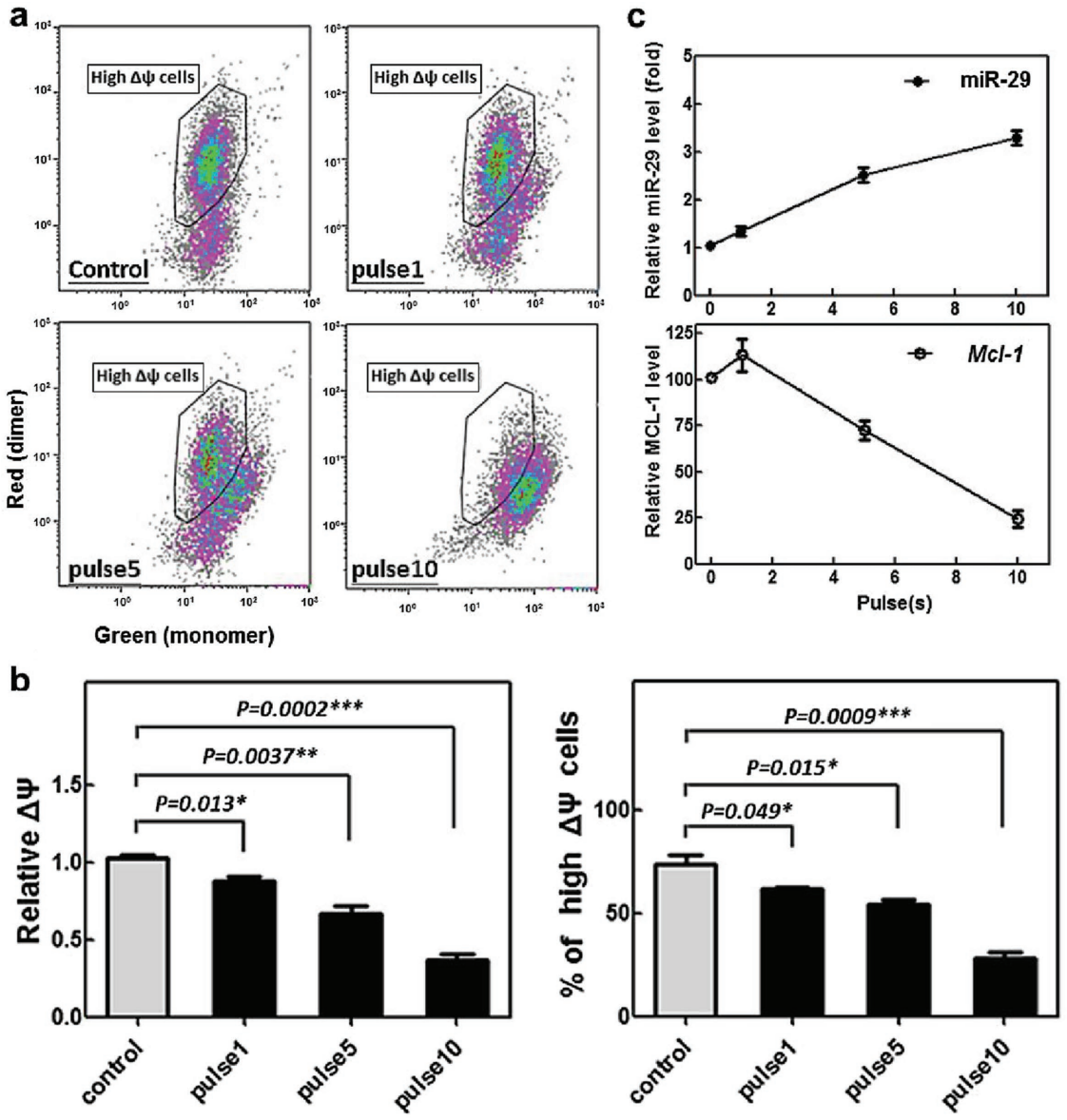

Figure 5. Controllable study of miR-29 dose-dependent treatment in primary mouse cardiomyocytes. a) The cardiomyocytes from adult mice were isolated and injected with miR-29 with different pulses (1, 5, 10. Pulse duration: 15 ms). The transfected cells were stained with JC-1 and analyzed by flow cytometry. The ratio of red (dimer)/green (monomer) reflected to the mitochondrial potential ($\Delta\Psi$). b) The dose-dependent reduction of $\Delta\Psi$ by miR-29 was observed. The percentage of high $\Delta\Psi$ cells was decreased by miR-29. c) The relative amount of intracellular miR-29b and *Mcl-1* mRNA was measured by real-time PCR, suggesting the positive correlation between pulse number and dose of miR-29.

with 1 cm^2 nanochannel array area, was diced from the whole wafer after etching.

The silicon based nanochannel chip was reproducible as the nanofabrication techniques, i.e., projection photolithography and DRIE, were robust with optimized protocols.

4.2. Microcap Array Pattern

The microcap array was made using SU-8 2015 (MicroChem), which was spun on the fabricated nanochannel array chip. The heights of microcaps were fixed at ≈5–10 μm. For alignment between microcap array and nanochannel array, a male "cross" marker was patterned and etched on the chip during the nanochannel etching process. A female "cross" marker on the photomask with the microcap array pattern was used to track the relative location between the microcap array feature and the nanochannel array on the chip. The alignment process and photolithography were performed on an automated UV-aligner (EVG 620). Every microcap feature in our design had an opening at the back-side, which was used to facilitate the entry of the cells when the liquids flow "through" the middle of the microcap.

4.3. "Dipping" for On-Chip Cell Trapping and Release

Prior to cell trapping, the chip patterned with microcap arrays was treated to be hydrophilic with Piranha solution (96% sulfuric acid, 120 °C) and oxygen plasma (PTS oxygen plasma system, US), and was exposed under UV-light for sterilization. Cells were

DOI: 10.1002/smll.201601465

transferred from cell culture medium to PBS solution, and then were transferred into a column glass tube (diameter: 1.5 cm; height: 5 cm) in a density of ≈1 million mL^{-1}. The chip, with the "U-shape" cup facing up, was then immersed into cell buffers and was held for ≈5 min (the chip was in an angle of 60°–90° to horizon). After the procedure of "dipping", the chip was steady and slowly lifted up (≈2 cm min^{-1}) using tweezers. One advantage of the procedure is that nearly all the cells that are not trapped could flow back to the cell buffer, allowing for high trapping specificity. Repeated "dipping-trap" was usually made in order to achieve a high capture efficiency. We note that the term "dewetting" in our experiments did not indicate the procedure of drying the chip surface, but the direction of the chip out of the cell buffer solution. In fact, a thin liquid film formed on the chip surface after "dewetting" and lasted for several minutes before vaporized. Such a time-duration gives enough time to perform on-chip electroporation.

After electroporation, the chip was transferred into 1 mL cell culture medium in a 6 well plate. A 200 µL pipette was used to gently wash the chip surface from the opposite direction to the cell trapping. As the opening of the microcap (as shown in the inset of Figure 1b) was designed for buffer flow through and cell release, the hydrodynamic force by pipette easily moved the cells out of the "U-shape" microcaps and floated back into the medium in an incubator (37 °C, 5% CO_2) for further applications.

4.4. High-Throughput Nanoelectroporation Platform

A bottom electrode was made from a glass slide (25 mm × 75 mm) coated with a gold layer (50 nm, Denton 520 evaporator). A PDMS spacer (width and length: 1 cm, thickness: 1 mm) was mounted on the gold-coated glass, forming a bottom chamber filled with cargo solution. After cells were trapped, the chip was gently placed on the bottom chamber. A top electrode (commercial electrode, Neon Transfection System) was moved to touch the buffer film on the chip surface in the connection as illustrated in Figure. 2d. A series of voltage pulses (voltage: 0–200 V, duration: 0–30 ms) were generated from a power supply (lab-made) for cellular electroporation. All components were sterilized with a 70% alcohol solution and UV-light.

For comparison, BEP was performed using a commercial system (Neon Transfection) and the operation was consistent with the instructions online. The MEP system used in cardiomyocytes transfection was based on a silicon 3D microchannel array chip. Each microchannel was 5 µm in diameter. Based on our previous research, 4 V was a safe voltage for cell electroporation.[29] In microchannel based electroporation, however, a sufficiently high voltage would cause irreversible cell membrane damage due to several reasons, including irreversible pore formation, pH change, thermal issues, etc.[10]

4.5. Cells Collection, Culture, and Transfection

MEFs were isolated from E12.5 embryos, and were cultured in Dulbecco's Modified Eagle's Medium (DMEM, Catalog no. 30-2002) with addition of 10% (v/v) fetus bovine serum (FBS, heat inactivated, Catalog no. 26010) and nonessential-amino acids. Mouse cardiomyocytes were isolated from adult mice, and were cultured in DMEM (Catalog no. 30-2002) with addition of 10% (v/v) FBS (heat inactivated, Catalog no. 26010) and nonessential-amino acids. FAM-ODNs (alpha DNA Co., Catalog no. 427520, excitation/emitting wavelength, 492/517 nm) were used to test the performance of nanoelectroporation in gene delivery, while PmaxGFP (3.5 kbp, Catalog no. VSC-1001, Amaxa Nucleofector Technology) was used to test the transfection performance. Hoechst (Sigma-Aldrich, Catalog no. 654434, excitation/emitting wavelength, 350/461 nm) was used to stain nuclei.

4.6. Image Acquisition and Data Analysis

As the silicon chip is nontransparent, imaging the on-chip cell trapping and FAM-ODN delivery was performed on an upright microscope (Leica DM2500). An inverted microscope (Nikon Eclipse Ti) was used to record fluorescent expressions of cells cultured off-chip. 3D cell-nanochannel image was reconstructed from slice-images by a fluorescence confocal microscope (Olympus FV1000).

COMSOL Multiphysics was used to analyze the electric field in both BEP and nanochannel electroporation systems.[34] The governing equation for the system (static electric field) used is: $\nabla \cdot (\sigma \nabla V) = 0$, where σ is the conductivity. The average length of the nanochannel is 13 µm, the diameter of nanochannel is 400 nm. Conductivities of extracellular fluid (PBS) and the cytosol are 0.8 and 0.2 S m^{-1}, respectively. The cellular membrane is estimated to be 5 nm thick with a conductivity of 5×10^{-7} S m^{-1}. In BEP system, the orientation of the cells and the number of cells (eight cells) are randomly generated.

The fluorescence data (e.g. intensity, cell counts) were analyzed using Nikon software (NIS Elements). High-throughput cell data (10 000 cells or higher) were analyzed by a flow cytometry (Beckman-Coulter, Brea, CA, USA).

4.7. RNA Extraction and Realtime PCR

Total RNA extraction was carried out by using Trizol (Invitrogen) and cDNA was made using random primers (Invitrogen, Life Technologies). Real-time PCR was performed by using TaqMan (Life Technologies) gene expression assay probe primer sets for miR-29b and *Mcl-1* by ViiA 7 Real-Time PCR System (Applied Biosystems, Grand Island, NY, USA). The expression of target genes relative to internal control gene was calculated using the threshold cycle number (C_t). The relative target gene expression for each condition was normalized to control and fold change determined using the comparative method ($2\Delta\Delta C_t$).

4.8. Mitochondrial Potential Measurement

After the transfection of miR-29b, the cardiomyocytes were stained with JC-1 to determine the mitochondrial membrane potential. JC-1 is a membrane-permeable lipophilic dye that acts as J-aggregates in the mitochondrial matrix (red fluorescence; 590 nm) and as monomers in the cytoplasm (green fluorescence, 529 nm). As mitochondrial depolarization happens, the red J-aggregates change to green monomers due to the loss of $\Delta\Psi$. Thus, mitochondrial $\Delta\Psi$ can be measured as an index of red (dimer)/green (monomer) fluorescence ratio. The stained cardiomyocytes were rinsed twice with media and analyzed with a flow cytometry (Beckman-Coulter, Brea, CA, USA).

DOI: 10.1002/smll.201601465

4.9. Statistical Analysis

Two-sided Student's *T*-test was used to determine the significance for data. The groups with p values ‹0.05 were considered statistically significant.

Supporting Information

Supporting Information is available from the Wiley Online Library or from the author.

Acknowledgements

L.C. and D.G.-P. contributed equally to this work. The authors are grateful to the National Science Foundation (EEC-0914790) and NIH (1R21EB017539-01A1) for supporting this study. The authors thank Dr. Zhaogang Yang for the suggestion on the concept of cardiomyocytes transfection.

[1] a) K. Kaji, K. Norrby, A. Paca, M. Mileikovsky, P. Mohseni, K. Woltjen, *Nature* **2009**, *458*, 771; b) J. Szczurkowska, A. W. Cwetsch, M. Dal Maschio, D. Ghezzi, G. M. Ratto, L. Cancedda, *Nat. Protoc.* **2016**, *11*, 399; c) M. dal Maschio, D. Ghezzi, G. Bony, A. Alabastri, G. Deidda, M. Brondi, S. S. Sato, R. P. Zaccaria, E. Di Fabrizio, G. M. Ratto, L. Cancedda, *Nat. Commun.* **2012**, *3*, DOI: 10.1038/ncomms1961.

[2] a) S. Meschini, M. Condello, P. Lista, B. Vincenzi, A. Baldi, G. Citro, G. Arancia, E. P. Spugnini, *Eur. J. Cancer* **2012**, *48*, 2236; b) Y. Sheng, L. Q. Chang, T. R. Kuang, J. M. Hu, *RSC Adv.* **2016**, *6*, 23279.

[3] L. Chang, J. Hu, F. Chen, Z. Chen, J. Shi, Z. Yang, Y. Li, L. J. Lee, *Nanoscale* **2016**, *8*, 3181.

[4] Z. G. Yang, L. Q. Chang, C. L. Chiang, L. J. Lee, *Curr. Pharm. Des.* **2015**, *21*, 6081.

[5] S. N. Wang, L. J. Lee, *Biomicrofluidics* **2013**, *7*, 11301.

[6] F. Liu, S. Heston, L. M. Shollenberger, B. Sun, M. Mickle, M. Lovell, L. Huang, *J. Gene Med.* **2006**, *8*, 1192.

[7] M. R. Prausnitz, V. G. Bose, R. Langer, J. C. Weaver, *Proc. Natl. Acad. Sci. USA* **1993**, *90*, 10504.

[8] a) W. Kang, J. P. Giraldo-Vela, S. S. P. Nathamgari, T. McGuire, R. L. McNaughton, J. A. Kessler, H. D. Espinosa, *Lab Chip* **2014**, *14*, 4486; b) M. Khine, A. Lau, C. Ionescu-Zanetti, J. Seo, L. P. Lee, *Lab Chip* **2005**, *5*, 38; c) T. Matsuda, C. L. Cepko, *Proc. Natl. Acad. Sci. U.S.A.* **2004**, *101*, 16; d) J. L. Pinyon, S. F. Tadros, K. E. Froud, A. C. Y. Wong, I. T. Tompson, E. N. Crawford, M. Ko, R. Morris, M. Klugmann, G. D. Housley, *Sci. Transl. Med.* **2014**, *6*, 233ra54.

[9] P. E. Boukany, A. Morss, W. C. Liao, B. Henslee, H. C. Jung, X. L. Zhang, B. Yu, X. M. Wang, Y. Wu, L. Li, K. L. Gao, X. Hu, X. Zhao, O. Hemminger, W. Lu, G. P. Lafyatis, L. J. Lee, *Nat. Nanotechnol.* **2011**, *6*, 747.

[10] N. Klauke, G. Smith, J. M. Cooper, *Anal. Chem.* **2010**, *82*, 585.

[11] W. E. Louch, K. A. Sheehan, B. M. Wolska, *J. Mol. Cell Cardiol.* **2011**, *51*, 288.

[12] M. A. Frias, M. C. Rebsamen, C. Gerber-Wicht, U. Lang, *Cardiovasc. Res.* **2007**, *73*, 57.

[13] J. Bokenes, I. Sjaastad, O. M. Sejersted, *J. Appl. Physiol.* **2005**, *98*, 1712.

[14] E. A. Woodcock, S. J. Matkovich, *Int. J. Biochem. Cell B* **2005**, *37*, 1746.

[15] a) C. Xie, Z. L. Lin, L. Hanson, Y. Cui, B. X. Cui, *Nat. Nanotechnol.* **2012**, *7*, 185; b) F. Santoro, S. Dasgupta, J. Schnitker, T. Auth, E. Neumann, G. Panaitov, G. Gompper, A. Offenhausser, *ACS Nano* **2014**, *8*, 6713; c) M. E. Spira, A. Hai, *Nat. Nanotechnol.* **2013**, *8*, 83; d) L. H. Hess, M. Jansen, V. Maybeck, M. V. Hauf, M. Seifert, M. Stutzmann, I. D. Sharp, A. Offenhausser, J. A. Garrido, *Adv. Mater.* **2011**, *23*, 5045; e) A. Q. Zhang, C. M. Lieber, *Chem. Rev.* **2016**, *116*, 215.

[16] K. Gao, X. Huang, C. L. Chiang, X. Wang, L. Chang, P. Boukany, G. Marcucci, R. Lee, L. J. Lee, *Mol. Ther.* **2016**, *24*, 956.

[17] K. Gao, L. Li, L. He, K. Hinkle, Y. Wu, J. Ma, L. Chang, X. Zhao, D. G. Perez, S. Eckardt, J. McLaughlin, B. Liu, D. F. Farson, L. J. Lee, *Small* **2014**, *10*, 1015.

[18] L. Q. Chang, P. Bertani, D. Gallego-Perez, Z. G. Yang, F. Chen, C. L. Chiang, V. Malkoc, T. R. Kuang, K. L. Gao, L. J. Lee, W. Lu, *Nanoscale* **2016**, *8*, 243.

[19] Y. Zhang, X. R. Huang, L. H. Wei, A. C. K. Chung, C. M. Yu, H. Y. Lan, *Mol. Ther.* **2014**, *22*, 974.

[20] A. Slusarz, L. Pulakat, *J. Cardiovasc. Med. (Hagerstown)* **2015**, *16*, 480.

[21] R. M. Perciavalle, D. P. Stewart, B. Koss, J. Lynch, S. Milasta, M. Bathina, J. Temirov, M. M. Cleland, S. Pelletier, J. D. Schuetz, R. J. Youle, D. R. Green, J. T. Opferman, *Nat. Cell Biol.* **2012**, *14*, 575.

[22] B. Lv, Z. H. Liu, S. P. Wang, F. B. Liu, X. J. Yang, J. T. Hou, Z. K. Hou, B. Chen, *Int. J. Clin. Exp. Pathol.* **2014**, *7*, 8542.

[23] N. Arnold, P. R. Koppula, R. Gul, C. Luck, L. Pulakat, *PLoS One* **2014**, *9*, e103284.

[24] a) M. Kawai, S. Kawashima, T. Sakoda, R. Toh, A. Kikuchi, K. Yamauchi-Takihara, K. Kunisada, M. Yokoyama, *Hypertension* **2003**, *41*, 956; b) M. Tatsuguchi, H. Y. Seok, T. E. Callis, J. M. Thomson, J. F. Chen, M. Newman, M. Rojas, S. M. Hammond, D. Z. Wang, *J. Mol. Cell Cardiol.* **2007**, *42*, 1137.

[25] a) A. M. Skelley, O. Kirak, H. Suh, R. Jaenisch, J. Voldman, *Nat. Methods* **2009**, *6*, 147; b) S. Kobel, A. Valero, J. Latt, P. Renaud, M. Lutolf, *Lab Chip* **2010**, *10*, 857.

[26] B. E. Henslee, A. Morss, X. Hu, G. P. Lafyatis, L. J. Lee, *Anal. Chem.* **2011**, *83*, 3998.

[27] a) L. Q. Chang, D. Gallego-Perez, X. Zhao, P. Bertani, Z. G. Yang, C. L. Chiang, V. Malkoc, J. F. Shi, C. K. Sen, L. Odonnell, J. H. Yu, W. Lu, L. J. Lee, *Lab Chip* **2015**, *15*, 3147; b) E. Salimi, M. Nikolic-Jaric, T. Cabel, K. Braasch, V. Jung, M. Butler, D. J. Thomson, G. E. Bridges, presented at *IEEE Proceedings of International Microwave Symposium, Seattle, June 2013,* **2013**, p. 403.

[28] P. Y. Chiou, A. T. Ohta, M. C. Wu, *Nature* **2005**, *436*, 370.

[29] L. Q. Chang, M. Howdyshell, W. C. Liao, C. L. Chiang, D. Gallego-Perez, Z. G. Yang, W. Lu, J. C. Byrd, N. Muthusamy, L. J. Lee, R. Sooryakumar, *Small* **2015**, *11*, 1818.

[30] S. Djurovic, N. Iversen, S. Jeansson, F. Hoover, G. Christensen, *Mol. Biotechnol.* **2004**, *28*, 21.

[31] W. K. Neu, J. C. Neu, in *Irreversible Electroporation*, (Eds: B. Rubinsky), Springer, Berlin, Heidelberg **2010**, p. 85.

[32] a) X. M. Huang, S. Schwind, B. Yu, R. Santhanam, H. Y. Wang, P. Hoellerbauer, A. Mims, R. Klisovic, A. R. Walker, K. K. Chan, W. Blum, D. Perrotti, J. C. Byrd, C. D. Bloomfield, M. A. Caligiuri, R. J. Lee, R. Garzon, N. Muthusamy, L. J. Lee, G. Marcucci, *Clin. Cancer Res.* **2013**, *19*, 2355.

[33] P. Bertani, W. Lu, L. Q. Chang, D. Gallego-Perez, L. J. Lee, C. Chiang, N. Muthusamy, *J. Vac. Sci. Technol. B* **2015**, *33*, 06F903.

[34] I. Zudans, A. Agarwal, O. Orwar, S. G. Weber, *Biophys. J.* **2007**, *92*, 3696.

Received: April 29, 2016
Revised: June 21, 2016
Published online:

DOI: 10.1002/smll.201601465